JOURNAL OF MATERIALS SCIENCE 24 (1989) 363–371

The influence of poly(acrylic acid) molecular weight on the fracture toughness of glass–ionomer cements

R. G. HILL*, A. D. WILSON, C. P. WARRENS
Laboratory of the Government Chemist, Department of Trade and Industry, Cornwall House, Waterloo Road, London SE1 8XY, UK

A linear elastic fracture mechanics approach has been used to characterize failure in glass–ionomer cements. The toughness, fracture toughness, flexural strength and inherent flaw size increase with the molecular weight of the poly(acrylic acid), whilst the Young's modulus remains approximately constant. The dependence of toughness on poly(acrylic acid) molecular weight is not as large as predicted by a reptation/chain pull out model for fracture and this is thought to be a result of the weak ionic crosslinks formed during the cement reaction.

1. Introduction

Glass–ionomer cements are formed by the reaction of poly(acrylic acid) PAA with an alumino–silicate glass [1]. The polyacid degrades the glass network releasing the aluminium and calcium ions and forming a silaceous gel. The PAA chains chelate the released cations and become crosslinked, forming a hard ceramic like cement which has many unusual properties. These novel cements have found use as a dental filling material and are currently being investigated for use as an orthopaedic bone cement.

The detailed chemistry and precise mechanism of the setting process in glass–ionomer cements has been reviewed by Wilson [2], but it is not fully understood. For our purposes, a glass–ionomer cement can be regarded as a glass filled PAA that is crosslinked by cations and plasticized by water. A previous study [3] investigated the influence of PAA molecular weight on the tensile strength of these cements. In these studies, both the PAA concentration and the molecular weight of the PAA were changed simultaneously, making interpretation of the results difficult. Furthermore, a diametral test was used to obtain the tensile strength, which must be considered suspect, since the calculation of the tensile strength from this testpiece assumes no plastic deformation and glass–ionomers are appreciably plastic, especially at low glass volume fractions, low PAA concentrations, and high molecular weights. Despite these criticisms the data from these studies do indicate an increase in tensile strength with molecular weight of the polyacid. The increase in tensile strength could arise from a reduction in the inherent flaw size, an increase in toughness or a combination of both these two parameters. Clearly these cements cannot be rigidly crosslinked, since if they were there would be no influence of the PAA chain length. In this respect [4] glass–ionomer cements behave like metal sulphonate and metal carboxylate ionomers, where the ionic crosslinks are not permanent, but break and reform after a characteristic lifetime.

It is worth point out at this stage that the term "glass–ionomer cement" is a misnomer. An ionomer is strictly speaking a hydrocarbon chain containing a small percentage of ionizable groups. Clearly PAA contains a very large proportion of ionizable groups. Thus, it can be dangerous to draw too many parallels between ionomers and glass–ionomer cements. Despite this, we will continue to use the term glass–ionomer, because it is now widely accepted for this category of material.

Dynamic mechanical thermal analysis of these cements show the presence of sharp loss peaks, typical of thermoplastics (Fig. 1). Thus, they are only weakly crosslinked and we will treat them as a type of thermoplastic polymer composite.

It is, therefore, worthwhile to summarize current thinking on the fracture of thermoplastic polymers.

2. Fracture of thermoplastic polymers

Berry's [5, 6] pioneering work on the fracture of thermoplastic polymers demonstrated that the measured fracture surface energy of a polymer was much greater than the energy required to break all the molecular chains crossing the crack plane. The high fracture surface energy was attributed to a localized flow process of the chain at the crack tip. Berry attributed the Griffith flaw size found with polymers, such as poly(methylmethacrylate) and polystyrene to a plastic zone or craze that formed prior to catastrophic failure.

Most polymers exist in the random coil conformation in the melt and the glassy state [7], thus, during deformation and fracture the chain has to be stretched prior to any chain scission occurring. Clearly, for this process to happen the chains must be securely held.

Present address: School of Materials Science and Physics, Thames Polytechnic, Wellington Street, London SE18 6PF, UK.

0022–2461/89 $03.00 + .12

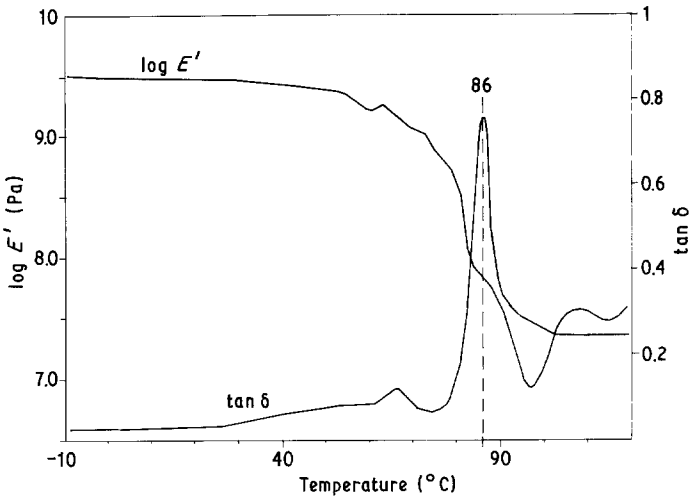

Figure 1 Storage modulus E' and tan δ for a glass–ionomer cement as a function of temperature. Note the sharp loss peak at 86° C typical of thermoplastics. (Experimental parameters: 1 Hz, strain = $\times 4$, 4° C min^{-1}, -10 g $k = 5.175$, single cantilever $1.61 \times 4.55 \times 14\,\text{mm}^3$).

There is general recognition that the strength of polymers is related to long range entanglements that serve to restrict chain motion. The early ideas of chain entanglements viewed the entanglement as a physical knot that served to severely restrict chain slippage during fracture. However, most chains are too inflexible for physical knots to occur and a model has been developed that views a chain as being trapped in a tube of entanglements formed by neighbouring chains [8]. This model, known as reptation, is shown schematically in Fig. 2. In the reptation model a chain is viewed as moving along an imaginary "tube" with a snake-like motion. The mobility of the polymer chain is constricted by the presence of entanglements, since in moving, one chain may not cross the contour of another. Longitudinal motion is also restricted by the interaction of substituents on neighbouring chains that give rise to potential barriers to chain mobility along the tube.

The dynamics of a polymer chain in a melt or concentrated solution have been described by the reptation model [9, 10]. This reptation model has also been used to describe fracture [11, 12] and crack healing [13, 14] in polymers. The reptation/chain pull out model for fracture is shown schematically in Fig. 3. The following analysis is based on that of Prentice [15].

Using a simple power law viscous model it can be shown that the shear stress (τ) experienced by the chain in its tube will be proportional to the apparent strain rate γ_a

$$\tau = \mu(\gamma_a)^n \tag{1}$$

where μ is a coefficient of viscosity resulting from the interaction between substituents on the extracted chain and the chains forming the tube. However

$$\tau = \frac{F}{A} \tag{2}$$

where F is the force acting on the end of the chain in the direction of the tube and A_s is the effective surface area of the tube occupied by the polymer chain

$$A_s = 2\pi rl \tag{3}$$

where r is the radius of the polymer chain, and l the

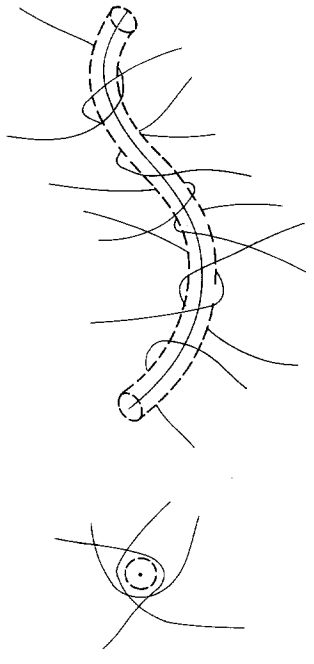

Figure 2 Schematic illustration of a polymer chain trapped in a tube of entanglements that gives rise to the reptation model.

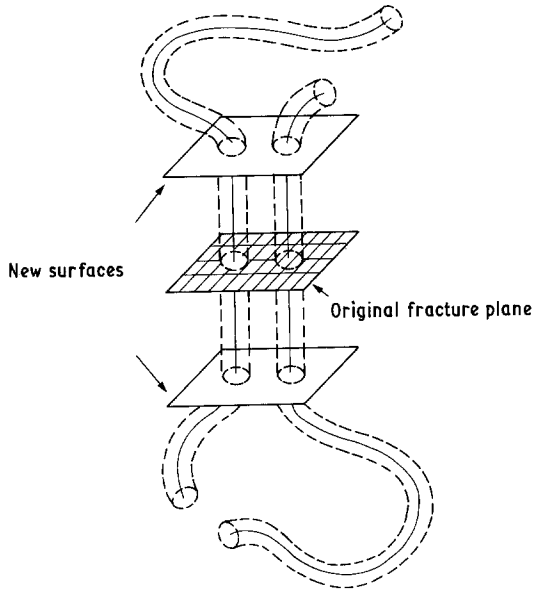

Figure 3 Fracture is assumed to take place as a result of the polymer chains being stretched then pulled out of their tubes in the fracture plane.

contour length of the tube occupied by the polymer molecule.

The apparent strain rate may be defined by

$$\gamma_a = \frac{V}{h} \quad (4)$$

where h is the spatial gap between the chain and the surface of its imaginary tube and V is the rate of removal of the chain.

Combining (1)–(4) we obtain

$$F = \mu 2\pi r \left(\frac{V}{h}\right)^n l \quad (5)$$

The energy to extricate one chain from its tube is then

$$\tau_0 = \int_{l=0}^{l=L} F \mathrm{d}l \quad (6)$$

where L is the total contour length of the tube vacated, thus

$$\tau_0 = \int_{l=0}^{l=L} \mu 2\pi r \left(\frac{V}{h}\right)^n l \mathrm{d}l \quad (7)$$

At constant v

$$\tau_0 = \mu \pi r \left(\frac{V}{h}\right)^n L^2 \quad (8)$$

The fracture surface energy per unit area of fracture plane will then be

$$\tau = \tau_0 N_s \quad (9)$$

where N_s is the number of segments crossing a unit area of crack plane. The assumption is that N_s is inversely proportional to the molecular cross-sectional area only. This assumption implies that a polymer chain only crosses the fracture plane once, which may be questionable, but considerably simplifies the analysis.

Combining Equations 8 and 9

$$\tau = \mu \pi r N_s \left(\frac{V}{h}\right)^n L^2 \quad (10)$$

The equation implies that at a fixed crack opening velocity (V) the work done in removing chains from a unit area of crack plane is proportional to the molecular weight squared

$$\tau \propto M^2 \quad (11)$$

At some stage a molecular weight will be reached where the stress to extricate a chain from its tube is greater than that required for homolytic chain scission of an extended segment.

A consequence of Equation 5 is that at a constant crack opening velocity a critical value of the force, F_c, will be reached at a critical chain length, l_c. Above this value of l_c the force required to pull out chains from their tubes will be greater than that to break the carbon–carbon bonds of the polymer backbone. Below this critical value (l_c) chain pull out will be the dominant mechanism and the fracture surface energy will be determined by Equation 10. Whilst above l_c chain scission will occur and the fracture surface energy will then be independent of molecular weight.

Equation 11 requires further slight modification to account for the fact that there is also a critical molecular weight, below which chains do not form entanglements. This results in the modification of Equation 11 to

$$\tau \propto (M - M_e)^2 \quad (12)$$

where M_e is the molecular weight required for entanglements to occur.

The critical molecular weight is the value above which chain scission occurs and the toughness is no longer related to molecular weight. The critical molecular weight is typically about 10^5, however its value is generally lower, where there are strong intermolecular interactions between polymer chains [16].

The entanglement molecular weight (M_e) again varies from polymer to polymer, but in general corresponds to between 100 and 300 monomer units [17]. The monomer unit molecular weight is 72 for PAA which gives an M_e of between 7000 and 21 000.

The application of a chain pull out model for the fracture of a glass–ionomer cement may be considered of doubtful value at first sight, however, preliminary observations indicate that the crack propagates through the PAA matrix phase and not through the glassy phase, thus fracture in glass–ionomer cements is essentially fracture of the polymer matrix phase.

3. Experimental

3.1. Materials

3.1.1. Poly(acrylic acid)s

The PAAs were supplied by Allied Colloids (Bradford, UK), these are coded E5, E7, E9, E11, E13 and E15. An additional high purity medical grade PAA was supplied by Dentsply (Weybridge, UK) and was given the code letters PF. All the PAAs were supplied as solutions, which were freeze dried and then ground in a vibratory mill. The fraction that passed through a 45 μm sieve was used in the preparation of the cements. The manufacturer's batch number and the nominal viscosity average molecular weights are listed in Table I, along with the number average ($\bar{M}_n$), weight average ($\bar{M}_w$) and z-average ($\bar{M}_z$) molecular weights determined by gel permeation chromatography (GPC). All the GPC molecular weights quoted are polyethylene oxide equivalent values. Typical molecular weight distributions are shown in Fig. 4.

3.1.2. Glasses

The composition of the glass powders A and B are listed in Table II. The glasses were finely ground with a maximum particle size below 45 μm. Both glasses

TABLE I Molecular weight details determined by gel permeation chromatography of poly(acrylic acid)s

Code	Batch number	$\bar{M}_n$	$\bar{M}_w$	PD	$\bar{M}_z$
E5	159	7.30×10^3	1.15×10^4	1.58	1.69×10^4
E7	AVS 228	1.13×10^4	2.27×10^4	2.01	5.93×10^4
E9	220	4.04×10^4	1.14×10^5	2.82	2.31×10^5
E11	415	1.12×10^5	3.83×10^5	3.42	6.13×10^5
E13	–	2.93×10^5	1.08×10^6	3.68	1.86×10^6
E15	012	1.30×10^5	1.49×10^6	11.50	2.85×10^6
PF	YG2	2.21×10^4	6.31×10^4	2.86	1.55×10^5

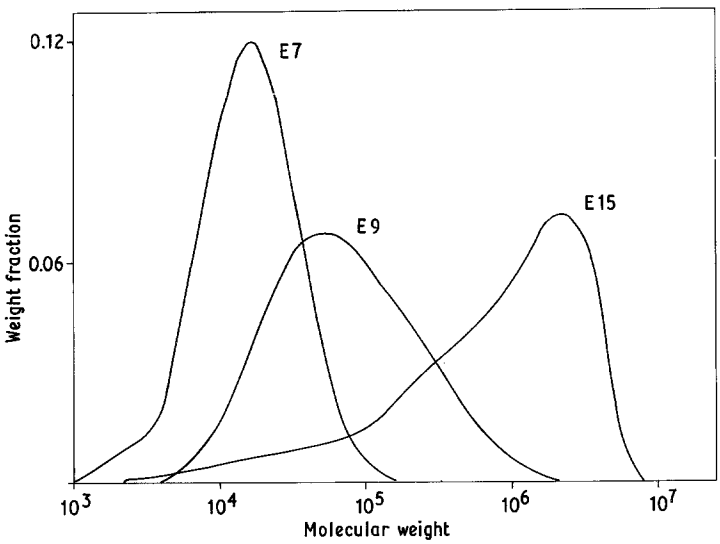

Figure 4 Molecular weight distribution of poly (acrylic acids). Note the pronounced low molecular weight tail of the high molecular weight material.

possess crystallites of corundum and fluorite, as well as possessing calcium rich amorphous droplets. The diameter of the droplets [18] was the order of 0.1 μm in glass A and the order of 1.0 μm in glass B.

3.1.3. Preparation of cements

Conventional glass–ionomer cements are made by mixing glass powder with aqueous PAA solutions. However, more recently water setting cements have been prepared. These consist of a mixture of glass powder, plus finely ground solid PAA which is mixed with water to form a cement. The commercial advantage of this approach is that it overcomes the problem of aqueous PAA solutions gelling in storage. Another advantage arises from the fact that the PAA particles have to dissolve in the added water prior to reacting; this slows the setting reaction to some extent and enables much higher molecular weight PAAs to be used.

The present study utilizes this approach to make relatively large double torsion (DT) and compact tension (CT) fracture toughness specimens of high molecular weight cements. Typically the polyacrylic acid (7 g) was blended with the glass powder (50 g). Batches of this mixture were then mixed with 10% m/m (+) tartaric acid solution. This is equivalent to a glass: water weight ratio of 2.22 : 1 and a PAA concentration of 31% m/m. This mixture was then placed in a mould consisting of two polished stainless steel plates and a stainless steel former (3.5 × 25 × 65 mm^3), coated with a thin layer of microcrystalline wax to prevent adhesion of the cement. The filled mould was compressed using two G clamps and excess cement paste eliminated.

TABLE II Glass composition

Component	Glass compositions	
	A	B
Si	12.39	13.45
Al	16.44	13.04
Ca	7.14	16.85
F	10.40	13.54
Na	7.26	0.81
P	4.54	1/75

This operation took about 4 min from start of mixing. The moulds were then placed in an oven at 37° C for 60 min. The set specimen blanks were then removed from the moulds and stored in water at 37° C for 23 ± 2 h.

Compact tension specimens were made in an identical fashion using stainless steel moulds with formers, measuring 3.0 × 24.0 × 25.0 mm^3. Holes were moulded into the specimen by means of two PTFE pins passing through the mould. Some cements could not be mixed on a large enough scale to make DT or CT specimen blanks. In these cases individual three-point bend specimens were made in stainless steel moulds measuring 3.0 × 3.0 × 30.0 mm^3.

A small number of samples were made with a higher glass content and polyacrylic concentration. To make these cements 10 g of PAA was mixed with 50 g of the glass powder. 12 g batches of this mixture were then mixed with 2.0 cm^3 of 10% m/m (+) tartaric acid solution. This is equivalent to a glass to water weight ratio of 5 : 1 and a PAA concentration of 50% m/m.

4. Test methods

4.1. The double torsion (DT) test

The DT test [19] has many advantages over other fracture toughness specimen geometries. The crack length is not required in the calculation of the stress intensity factor, since the DT geometry makes it a linear compliance testpiece. It can be used to investigate crack stability in a material, affording an insight into the fracture process. Providing cracks are stable the testpiece can be used to obtain crack velocity–stress intensity factor diagrams, from which static fatigue lifetimes can be predicted. The crack propagates at constant velocity down the DT specimen, the velocity being determined by the crosshead displacement rate, the specimen dimensions and the modulus of the material. The specimens are easy to manufacture and blunt cracks can readily be detected. Finally, after fracturing, the large DT specimens can be cut down to make three-point bend specimens, making economical use of materials and resources.

DT specimens 3.5 × 65 × 25 mm^3, Fig. 5 were produced as described previously in the form of

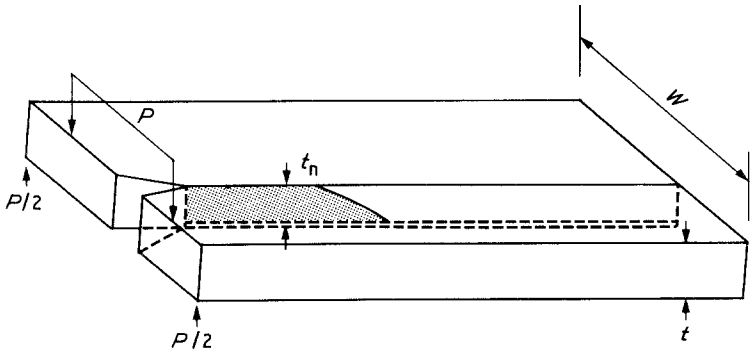

Figure 5 A double torsion specimen.

rectangular plates. A sharp groove 0.5 mm deep was cut down the centre of the specimen using a microslice cutter (Microslice 11 Metals Research Ltd, Cambridge, UK). A slot was cut at one end of the specimen, into which was pressed a scalpel blade.

The DT test was performed using an Instron electromechanical testing machine (Instron Ltd, High Wycombe, UK). During the test the specimen was supported on two parallel rollers of 3 mm diameter and spaced 20 mm apart and load applied at a constant rate (0.1 mm min^{-1}) to the slotted end via two 3 mm diameter ball bearings spaced 10 mm apart. The specimen was therefore subjected to four-point bend loading, during which the crack initiated and propagated, along the centre of the specimen, within the groove. The test was carried out in tap water at 37 ± 2° C. The groove depth was chosen to eliminate crack shape corrections [20].

In a DT test the mode I stress intensity factor K_I is independent of crack length and is given by [21]

$$K_I = P_c W_m \left(\frac{3(1 + \nu)}{Wt^3 t_n}\right)^{1/2} \quad (13)$$

where W_m is the moment arm, W the specimen width, t the specimen thickness, t_n is the thickness in the crack plate and ν Poisson's ratio (assumed to be 0.33). Values for K_I, the fracture toughness, were obtained by substituting the appropriate specimen dimensions along with the load at fracture P_c in Equation 13. Typical load–deflection plots are shown in Figs 6 and 7 for stable and unstable "stickslip" crack growth.

4.2. The compact tension (CT) test

The compact tension test piece was a miniature version of the one described in BS 5447. The value of W was reduced to 20 mm and the specimen thickness was reduced from 0.5 to 0.3 W (Fig. 8).

The specimen blanks were cut along the dashed line (Fig. 8) using an edge coated diamond flitting wheel such that the final length of the saw cut was between 0.45 and 0.55 W. The length of the fine saw cuts were measured after testing. The specimens were then tested quasi-statically in an Instron testing machine using a crosshead velocity of 0.1 min^{-1}. All tests were carried out in tap water at 37 ± 2° C. The Gurney–Hunt sector [23] area method could not be applied due to the opacity of the cements. Instead the total area under the curve was used to calculate the toughness (G_I).

The maximum load at fracture (P_c) and the sawcut length (a) were substituted into Equation 14 to give the mode I stress intensity factor (K_I)

$$K_I = \frac{P_c}{tW^{1/2}}(Y) \quad (14)$$

where

$$Y = 29.6\left(\frac{a}{W}\right)^{1/2} - 185.5\left(\frac{a}{W}\right)^{3/2} + 655.7\left(\frac{a}{W}\right)^{5/2} - 1017\left(\frac{a}{W}\right)^{7/2} + 638.9\left(\frac{a}{W}\right)^{9/2}$$

4.3. The flexural test

Immediately after testing the DT specimens, the broken halves were cut up into three-point bend specimens, measuring 3.0 × 3.5 × 30 mm^3. In a three-point bend specimen the relationship between the applied load (P) and the deflection at the centre of the specimen

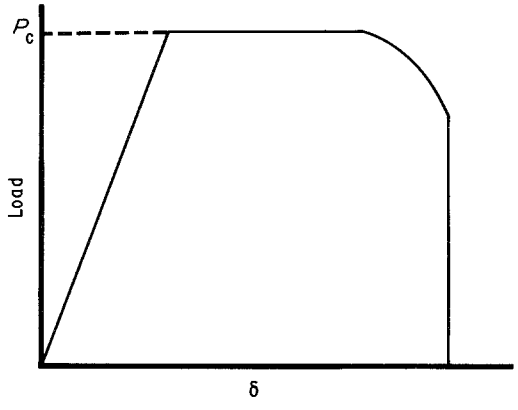

Figure 6 A typical load–deflection plot for a double torsion specimen undergoing stable crack growth.

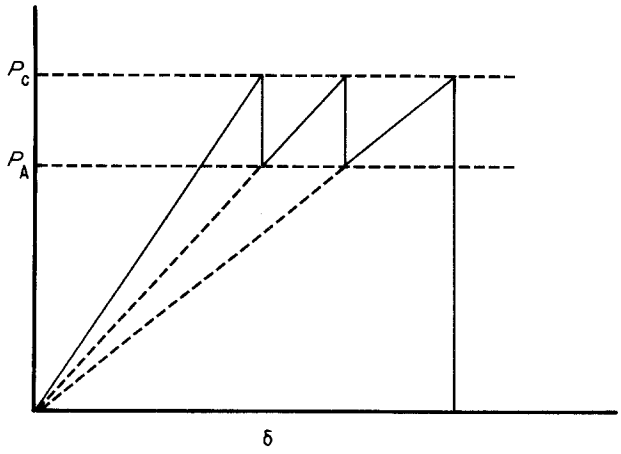

Figure 7 A typical load–deflection plot for a double torsion specimen undergoing unstable "stick slip" crack growth.

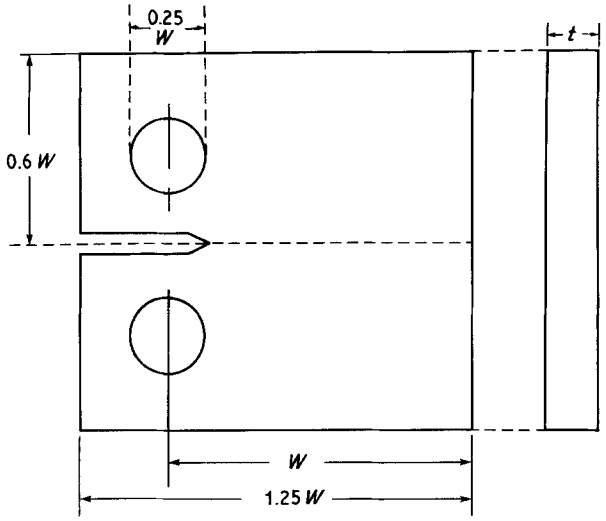

Figure 8 A compact tension specimen.

(δ) for a specimen of rectanglar cross section is given by

$$P = \frac{4\delta Ebt^3}{s^3} \quad (15)$$

where t is the beam thickness, b the beam width and s the span. A span of 20 mm was used, with a crosshead displacement rate of 0.1 mm min^{-1}. This gives an almost identical strain rate to that used in the DT tests. All tests were carried out in tap water at 37 $\pm$ 2° C. The Young's modulus was calculated from the initial slope of the load deflection plot. The unnotched fracture strength is defined by

$$\sigma_f = \frac{3Ps}{2bt^2} \quad (16)$$

A minimum of five specimens were tested for each test condition. Any specimens that were not visually flaw free were discarded prior to testing.

4.4. Calculation of the strain energy release rate (G_1) from DT specimens

The strain energy release rate was calculated assuming that pure linear elastic fracture mechanics apply using the following expression

$$G_1 = \frac{K_1^2(1 - v^2)}{E} \quad (17)$$

The value for E was taken as 1565 MNm^{-2} which is the mean value for all the cements tested with the low glass content and low PAA concentration mix. It is implicitly assumed that for reasonable molecular weights the Young's modulus will be independent of polymer chain length.

4.5. Calculation of the Griffith flaw size

A linear elastic fracture mechanics approach was used to calculate the inherent flaw size. The value of the inherent flaw size gives an estimate of the size of microstructural features, or defects which limit the strength of a material in the absence of an external flaw or crack. Sharp flaws larger than the inherent flaw size will reduce the strength of the material. The method used for the calculation of the inherent flaw size is based on the Irwin relation, which is applicable to the geometry and loading of a bend type single edge notch specimen first used by Brown and Strawley [24]

$$K_1 = Y\frac{6m}{tw^2}(a)^{0.5} \quad (18)$$

where m is the bending moment equal to $PS/4$ and Y is a geometrical calibration factor, which in the absence of an external flaw or crack, assumes a value of 1.93.

The Irwin relation can be written in terms of the fracture toughness (K_1): the unnotched fracture strength (σ_f) and the flaw size (a^*)

$$a^* = \left(\frac{K_1}{Y\sigma_f}\right)^2 \quad (19)$$

5. Results and discussion

Tables III and IV summarize the results of the molecular weight study. There is a reasonable correlation between the DT and CT tests for the fracture toughness (K_1), a linear regression analysis giving a correlation coefficient r = 0.950. There is also reasonable agreement between the two sets of values for the strain energy release rate (G_1) with a correlation coefficient, r = 0.998. The agreement between the two sets of data is not ideal, but is sufficient to substantiate the validity of the linear elastic fracture mechanics approach to these brittle materials. No edge effects, for example shear lips, were found on any of the fracture surfaces, further supporting the validity of the testing techniques. Characteristic "fish tail" markings were observed on the fracture surface of the CT specimens. Such markings are common with thermoplastic polymers. All the cements gave slow stable crack growth. Typical load–deflection plots obtained with

TABLE III The influence of PAA molecular weight on fracture toughness and flaw size (glass A)

Code	$\bar{M}_w$	DT values				CT values			
		K_1 (MN m$^{-3/2}$)	SD (n = 5)	G_1 (J m^{-2})	a^* (μm)	K_1 (MN m$^{-3/2}$)	SD (n = 5)	G_1 (J m^{-2})	a^* (μm)
E5	1.15 × 10^4	0.13	0.01	10	91	0.13	0.01	13	91
E7	2.27 × 10^4	0.16	0.01	15	106	0.14	0.02	15	81
E9	1.14 × 10^5	0.23	0.02	30	142	0.17	0.02	26	78
E11	3.83 × 10^5	0.26	0.02	38	171	0.20	0.02	36	101
E13	1.08 × 10^6	0.33	0.04	61	155	0.23	0.05	47	75
E15	1.49 × 10^6	–	–	–	–	0.25†	–	53†	96
PF	6.31 × 10^4	0.22	0.01	28	121	0.20	0.02	23	103

† 1 specimen only; a^* flaw size.

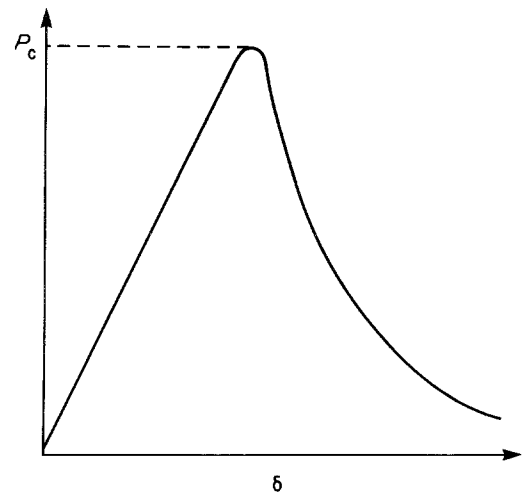

Figure 9 A typical load–deflection plot for a compact tension specimen.

the DT and CT tests are shown in Figs 6 and 9 respectively. In general, slow stable crack growth is found in thermoplastic polymers where the crack propagates through a well defined process zone, for example, a craze or plastic zone. Stable cracks occur when

$$\frac{dG_1}{da^0} > 0$$

where a^0 is the crack velocity. Unstable crack propagation generally occurs in thermosets, for example, epoxy resins where

$$\frac{dG_1}{da^0} < 0$$

There is a clear increase in fracture toughness (K_1), toughness (G_1), and unnotched fracture strength (σ_f) with molecular weight for both the DT and CT tests.

However, the flaw size (a^*) increased with the molecular mass when calculated from DT tests but not from CT tests. The DT values for a^* are thought to be the more reliable, since this test does not involve the measurement of crack length.

Thermoplastic polymers (except at very low molecular weight, where free volume becomes important)

TABLE IV The influence of PAA molecular weight on flexural strength and Young's modulus (glass A)

Code	$\bar{M}_w$	σ_f (MN m^{-2})	SD (n = 5)	E (MN m^{-2})	SD (n = 5)
E5	1.15×10^4	7.06	1.05	1750	314
E7	2.27×10^4	8.05	0.61	1754	374
E9	1.14×10^5	9.99	0.85	1487	173
E11	3.83×10^5	10.30	1.66	1242	259
E13	1.08×10^6	13.74	0.57	1429	132
E15	1.49×10^6	13.25	1.90	1580	145
P.F.	6.31×10^4	10.22	0.92	1714	104

exhibit moduli that are independent of molecular weight [16]. Crosslinking a polymer normally results in a dramatic rise in the Young's modulus. The experimental scatter on the Young's modulus data is greater than expected and probably arises due to slight misalignment of the specimens in the testing jig. However, the modulus (E) as expected on theoretical grounds, appears to be independent of the PAA molecular weight. The approximately constant moduli of these cements, therefore, indicates that the chemistry of the setting process is unaffected by the molecular weight of the PAA used to make the cement. Further corroboration that the molecular weight of the PAA has no influence on the setting process is shown in Table V, where a higher glass content and polymer concentration were used; here again, the moduli remain constant as the molecular weight is varied. The clear influence of molecular weight is surprising considering the overlapping molecular weight distributions shown in Fig. 4. Results from a previous study using the radically different glass B, show a similar influence of the PAA molecular weight. There is a good correlation between the two sets of data (Fig. 10) which again indicates that molecular weight affects the physics of the failure process, but not the chemistry of the setting process.

The values for log (G_1) calculated from the CT test data are plotted against both log ($\bar{M}_n$) and log ($\bar{M}_w$) in Fig. 11 and are compared with the expected behaviour from the reptation model. The slope predicted from the theory is drawn as a broad line, since the entanglement molecular weight is not known precisely for PAA. A very similar plot was obtained with DT

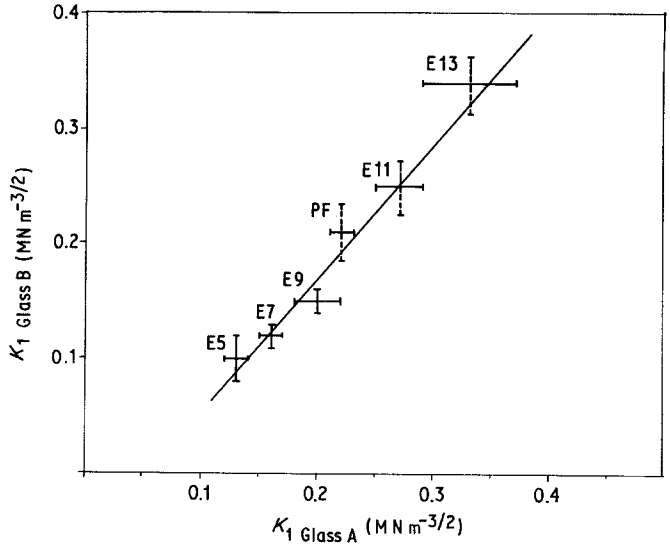

Figure 10 Plot of K_1 for glass B against K_1 for glass A. (⊢—⊣ 2 × SD (n = 5), ⊢- - -⊣ 2 × estimated SD).

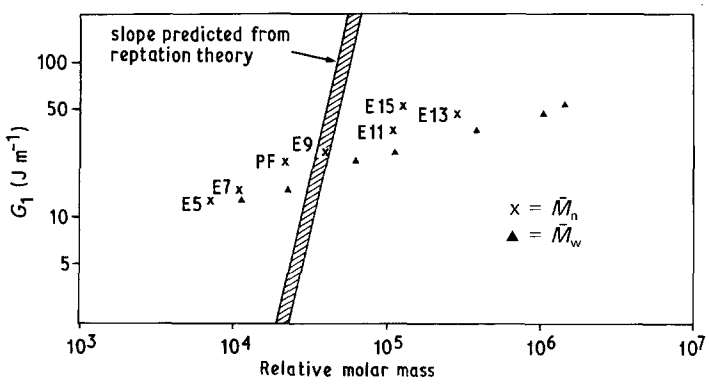

Figure 11 Plot of log (G_1) determined using the CT test against log ($\bar{M}_n$) (x) and log ($\bar{M}_w$) (▲). The shaded line indicates the slope expected from reptation theory.

test data. The reptation model is only strictly valid for monodisperse polymers and cannot take into account polydispersity. However, the model does predict negligible toughness for polymers below their entanglement molecular weight and the cement based on the PAA E5 clearly exhibits significant toughness. The molecular weight of the E5 would be expected to be close to the entanglement value.

The rate of increase in the toughness with the PAA molecular weight is not as large as predicted by the chain pull-out theory. At very high molecular weights the toughness should be independent of the polymer chain length and, therefore, the effect of polydispersity can largely be ignored. Results for the toughness of poly(methyl methacrylate) as a function of molecular weight are shown in Fig. 12. The plot of log (G_1) against log ($\bar{M}_w$) gives a slope slightly greater than the theoretical value of 2.0 compared with a slope of less than 1.0 found for the glass–ionomer cements. Furthermore, the magnitude of the toughness at very high molecular weights compared with low molecular weights is much greater for poly(methylmethacrylate) than for glass–ionomer cements. The case of the observed slope being shallower than the predicted one is unlikely to be the result of polydispersity in chain lengths. The most likely explanation for this failure of the chain pull-out model is that interchain crosslinking by cations occurs to a significant extent. Clearly the ionic linkages are not so strong that failure always occurs by chain scission and not so weak that failure occurs only by chain pull-out, with the length of the chain entirely determining the toughness. At low molecular weight the cooperative effect of the ionic linkages, plus no doubt other interchain bonds, serves to increase the effective molecular weight in the cement and increase the toughness. At high molecular weights these interchain bonds serve to promote chain scission. Clearly if the crosslinks play a significant role the chain pullout model will not apply.

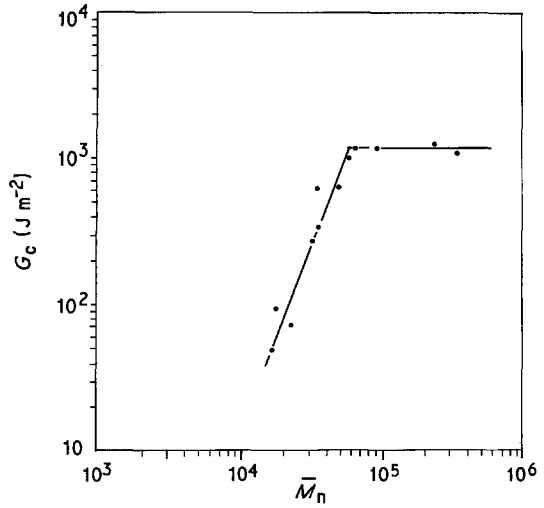

Figure 12 Dependence of toughness on molecular weight for the thermoplastic poly(methylmethacrylate) (taken from [15]). Slope = 2.45.

The flexural strength does not increase above a weight average molecular weight of 1.08×10^6 indicating that cement properties are now probably independent of molecular weight.

The flaw size (Table III) increases with the molecular weight of the PAA. In many polymers it is recognized that the inherent flaw size corresponds to a plastic zone, or craze that forms, just prior to fracture. The flaw size is considerably larger than the maximum glass particle size, which is the order of 40 μm. If the flaw size corresponded to a defect, for example, a surface crack, then a much greater scatter on the flexural strength values would be expected, since such flaws would have a statistical chance of being present in the small area of high stress on the tensile edge of the three-point bend specimens.

Possibly in the high molecular weight cements, the flaw size corresponds to undissolved PAA particles, but if this was the case a constant flaw size for the low molecular weight cements would be expected. Furthermore, the flaw size is somewhat larger than the PAA particle size. To confirm that the PAA particles were dissolving completely two sets of samples were made with the same PAA concentration and the same glass content, one set was made using a freeze dried PAA and the other using an aqueous PAA solution. The results are shown in Table VI and both methods of specimen manufacture give approximately identical values indicating that the PAA particles dissolve completely.

Small amounts of plastic deformation were observed on the load deflection plots from three-point bend

TABLE V The effect of PAA molecular weight on the flexural strength and Young's modulus of high glass content (glass A) cements

	$\bar{M}_w$	σ_f (MN m^{-2})	SD (n = 5)	E (MN m^{-2})	SD (n = 5)
E5	1.15×10^4	13.92	0.96	7423	274
E7	2.27×10^4	23.00	3.53	7783	657
PF	6.31×10^4	30.70	3.30	7526	363

TABLE VI Comparison of freeze dried and aqueous methods of specimen fabrication for glass A and PF polyacrylic acid

Method of preparation	K_I ($MN\,m^{-3/2}$)	SD ($n = 5$)	G_I ($J\,m^{-2}$)	σ_F (μm)	SD ($n = 5$)	E (MNm^{-2})	SD ($n = 5$)	a^* (μm)
Aqueous	0.20	–	17†	10.53	0.57	2337	207	96
Freeze dried	0.22	0.01	28	10.22	0.92	1714	106	124

† Modulus taken as 2337 in the calculation of G_I.

specimens of cements, based on high molecular weight PAAs just prior to catastrophic failure, whilst cements based on low molecular weight PAAs exhibited a more brittle failure. Small amounts of plastic deformation prior to failure are found with many polymers and are indicative of the formation of localized plastic zone or craze, through which subsequent crack propagation takes place.

The cements studied in this paper have low glass contents and low PAA concentrations compared to the cements used commercially. Higher glass contents and polymer concentrations might be expected to favour crosslinking and thereby reduce the effect of molecular weight. Cement pastes with high glass contents and PAA concentrations could not be mixed satisfactorily on a large enough scale to make DT or CT specimens, however, the smaller flexural strength specimens could be made. The results are shown in Table V. There is again a clear influence of PAA molecular weight, thus there is little evidence of increased crosslinking leading to a reduction in the influence of PAA chain length.

The higher Young's modulus found for the cements mixed at high glass contents and PAA concentrations probably arises for a combination of reasons, including: an increased volume fraction of residual glass particles, an increased density of crosslinks in the form of ionic linkages and entanglements, and a reduction in the unbound water content of the cement. Free unbound water molecules are likely to have a plasticising action in set cement pastes.

6. Conclusions and implications

The increase in toughness with PAA molecular weight is not as large as predicted by the chain pullout theory. However, molecular mass does have a pronounced effect and although the model is quantitatively incorrect it does predict many of the effects observed. The quantitative analysis of the data would be considerably improved by the use of sharp molecular weight fractions. Further data on the fracture toughness of cements with high glass contents and PAA concentrations similar to those found commercially would be useful. The flaw size and toughness might be expected to fall as the density of crosslinks is increased.

Cracks are inherently stable in these cements and the indication is that the crack probably propagates through a well defined plastic zone or craze. Therefore the study of the development of this zone may well be rewarding.

During the last few years, there has been considerable interest in the so-called "macrodefect free cements" which are polymer modified Portland cements. There are certain similarities between these cements and glass–ionomer cements [25]. Though they only contain a few percent of polymer these cements also exhibit loss peaks typical of thermoplastic polymers and the application of an identical approach to that outlined in this paper may be useful in understanding the controversial role of the polymer component in these cements.

References

1. S. CRISP and A. D. WILSON, *J. Appl. Chem. Biotechnol.* **23** (1973) 811.
2. A. D. WILSON, *Brit. Polym. J.* **6** (1974) 165.
3. S. CRISP, G. ABEL and A. D. WILSON, *J. Dent.* **5** (1977) 117.
4. A. E. GONZALEZ, *Polymer* **25** (1984) 1469.
5. J. P. BERRY, *J. Polym. Sci.* **50** (1961) 313.
6. *Idem, S. P. E. Trans.* **1** (1961) 1.
7. R. N. HOWARD, "The Physics of Glassy Polymers", Applied Science Publishers, London (1973).
8. S. F. EDWARDS, *Proc. R. Soc. London* **92** (1969) 9.
9. P. G. DE GENNES, "Scaling Concepts in Polymer Physics", Cornell University Press, New York (1979).
10. *Idem, Physics Today*, June (1983) 344.
11. P. PRENTICE, *Polymer* **24** (1983) 344.
12. G. L. PITMAN and I. M. WARD, *ibid.* **20** (1979) 895.
13. K. JUD, H. H. KAUSCH and J. G. WILLIAMS, *J. Mater. Sci.* **16** (1981) 204.
14. H. H. KAUSCH and K. JUD, *Plast. Rubber Process. Appl.* **2** (1982) 265.
15. P. PRENTICE, *J. Mater. Sci.* **20** (1985) 1445.
16. R. J. MARTIN, J. F. JOHNSON and A. R. COOPER, *J. Macromol. Sci. Rev. Macromol. Chem.* **C8** 57.
17. J. D. FERRY, "Viscoelastic Properties of Polymers", 3rd Edn, Wiley, New York (1980).
18. T. I. BARRY, R. P. MILLER and A. D. WILSON, XI Conference on the Silicate Industry, Budapest, May (1973) pp. 881–893.
19. D. P. WILLIAMS and A. G. EVANS, *J. Test. Eval* (1973) 264.
20. P. S. LEEVERS and J. G. WILLIAMS, *J. Mater. Sci.* **20** (1985) 77.
21. J. A. KIES and B. J. CLARKE, "Fracture", edited by P. L. Pratt (Chapman and Hall, London, 1969) p. 483.
22. BS 5447, "Plane Strain Crack Toughness, K_{IC} Testing of Metallic Materials, British Standards Institute (1977).
23. C. GURNEY and J. HUNT, *Proc. R. Soc. London* **A299** (1967) 508.
24. W. F. BROWN and J. E. STRAWLEY, ASTM STP 410 (American Society for Testing and Materials, Philadelphia, 1965) p. 13.
25. S. A. RODGERS, S. A. BROOKS, W. SINCLAIR, G. W. GROVES and D. D. DOUBLE, *J. Mater. Sci.* **20** 2853 (1985).

Received 10 December 1987
and accepted 29 April 1988